Title

Estimating fruit tree growth curves in breeding field using fragmented longitudinal data: An application to citrus hybrid seedlings

Running title: Estimating growth curves in citrus seedlings

Authors

Soh Kimura[1], Mai F. Minamikawa[2], Keisuke Nonaka[3], Tokurou Shimizu[3, 4], Hiroyoshi Iwata[1*]

[1]Laboratory of Biometry and Bioinformatics, Department of Agricultural and Environmental Biology, Graduate School of Agricultural and Life Sciences, The University of Tokyo, 1-1-1 Yayoi, Bunkyo, Tokyo 113-8657, Japan

[2]Institute for Advanced Academic Research (IAAR), Chiba University, 1-33 Yayoi, Inage, Chiba, Chiba 263-8522, Japan

[3]Institute of Fruit Tree and Tea Science, NARO, Okitsu Nakacho, Shimizu, Shizuoka 424-0292, Japan

[4]Laboratory of Plant DNA Analysis, Kazusa DNA Research Institute, 2-6-7 Kazusa-kamatari, Kisarazu Chiba, 292-0818 Japan

*To whom correspondence should be addressed:

Email: hiroiwata@g.ecc.u-tokyo.ac.jp

Tel: +81-03-5841-5069

The official email addresses of other authors:

Soh Kimura[1]: kimura@ut-biomet.org

Mai F. Minamikawa[2]: minamikawa@chiba-u.jp

Keisuke Nonaka[3]: nonakak6@affrc.go.jp

Tokurou Shimizu[3]: tshimizu@affrc.go.jp

Abstract

Vegetative and reproductive growth in fruit trees is interconnected, and analyzing this relationship can provide valuable insights into fruit quality. However, characterizing vegetative growth through growth models is challenging because of the difficulty in obtaining longitudinal data, given the slow growth rate. In breeding fields, in contrast, seedlings of different ages are planted, allowing for simultaneous measurements that yield a dataset resembling longitudinal data with missing values --termed "fragmented longitudinal data." Because longitudinal data are obtained from a single measurement, they can potentially shorten the period required for growth curve estimation. Bayesian nonlinear models offer advantages in estimating curves from incomplete data. In this study, we generated fragmented longitudinal data using genome data with 45,929 markers from 624 citrus hybrid seedlings and applied a Bayesian nonlinear model to explore its potential. We also incorporated genomic information into the model to assess the impact of the estimation accuracy. Our simulations indicated that the Bayesian nonlinear model's ability to interpolate missing values significantly improved the estimation performance. At best, the mean square error of the parameter characterizing the later growth stage was reduced by 84.3 mm^2. Although the improvement from incorporating genomic information was modest, it still surpassed models that lacked genomic data. We also predicted the curves of untested individuals using the estimated parameters. Although the prediction accuracy of each parameter measured by the correlation coefficient was lower than 0.5, one parameter consistently showed a better accuracy. Further research is required to reveal the advantages of integrating genomic data for better predictions.

Introduction

Vegetative growth in fruit trees is closely linked to reproductive growth, acting as both a source and sink. Understanding this relationship has been a key focus for researchers because it directly influences fruit quality[1]. While physiological research has traditionally dominated the study of this relationship[2,3], quantitative analysis of vegetative traits, such as trunk diameter and crown width, along with subsequent correlation studies, has highlighted the significant role of vegetative growth in determining fruit quality[4–7]. Additionally, these traits have been shown to correlate with the juvenile period and inbreeding depression[8–10]. With the advent of next-generation sequencing, these analyses are expected to expand to the genetic level. However, the complex growth patterns of trees and the dynamic nature of their phenotypes over time make the genetic analysis of these traits highly time-dependent. Therefore, it is essential to evaluate the evolving growth patterns and align genetic analyses accordingly.

The coexistence of trees of different ages in the same field presents specific challenges for genetic analyses, particularly for traits that are strongly influenced by time. In fruit tree breeding, orchards often contain a mix of candidates selected at various growth stages. For instance, in Japanese Citrus breeding, approximately 1,000 seedlings obtained from various crosses are grafted onto trifoliate orange rootstocks annually and assessed for over 20 traits, including fruit quality and disease resistance[11,12]. Given that selection periods are typically under 8 years and new seedlings are planted annually, breeding orchards contain trees of diverse ages from various crosses. To analyze genetic variations in trees of various ages simultaneously, it is necessary to link data from different growth stages using a growth model and evaluate their growth patterns based on the parameters of that model.

Growth models such as the logistic and Gomperz models are effective in describing tree growth trajectories using a minimal number of time-independent parameters[13]. Their nonlinearity

allows them to outperform linear models, such as polynomial regression, in terms of requiring fewer interpretable parameters and providing more stable extrapolation[14], which has led to extensive studies evaluating their applicability[15]. Growth models have been used to better understand growth patterns of fruits[16]. The parameters estimated from these models, which serve as time-independent indices of growth, are often used as target traits for genomic selection[17,18] or genome-wide association study (GWAS)[19,20]. Prior research has highlighted both the challenge of analysis based on time-dependent indices and the potential of the growth model, proposing QTL analysis based on stage-dependent indices derived from these models[21]. Unlike cross-sectional data, which can be obtained from a single measurement, longitudinal data, which are necessary for estimating growth curves, require repeated sampling, placing a significant burden on researchers. This burden is particularly high for trees, which have slow growth rates and require measurements over several years. Recently, unmanned aerial vehicles (UAVs), such as drones, have been used to measure phenotypic data and show promise in reducing this burden[22,23]. However, despite the anticipated reduction in measurement load owing to advancements in UAV technology, acquiring longitudinal data will continue to be challenging owing to the time required.

The use of an age-mixed field along with nonlinear mixed-effect models (NLMEMs) and Bayesian nonlinear models offers a potential solution for this challenge. In an age-mixed field, trees of different ages are planted together, allowing for simultaneous measurement of all individuals. This results in a dataset similar to longitudinal data, which we refer to as “fragmented longitudinal data.” Although these data contained substantial missing values for each tree (genotype), they were collected over a relatively short time span. If accurate growth curves can be estimated from these fragmented longitudinal data, the overall measurement time can be significantly reduced.

The nonlinear mixed effect model (NLMEM), which combines the characteristics of a

nonlinear model and a mixed-effect model, is frequently employed in the literature to handle incomplete longitudinal data[24,25]. NLMEM includes both fixed and random effects, where fixed parameters are shared among all subjects and random parameters are unique to each individual[26]. Because individual-specific values of random parameters are estimated based on a covariance structure derived from all individuals in the dataset, each individual tree (genotype) can "borrow" information from the others, allowing for the imputation of missing values[13]. Bayesian nonlinear mixed models extend NLMEMs by assuming that all model parameters, not only random effects, follow specific distributions[27], which further aid in imputing missing values[28]. Therefore, we expect that NLMEM and Bayesian nonlinear modeling will play crucial roles in estimating growth curves from fragmented longitudinal data. Recent studies have incorporated genomic information into these models[29,30]. As growth parameters are genetically controlled to some extent, incorporating genomic information into these models may improve parameter estimation accuracy. Moreover, when genomic information is considered, the growth curves of untested individuals can be predicted based on genomic data in the context of genomic prediction and selection[31].

In this study, we applied Bayesian nonlinear models to estimate growth curve parameters using fragmented longitudinal data collected from age-mixed fields without the need for time-consuming, labor-intensive repeated measurements. In addition, we evaluated whether incorporating genomic information into the models could improve the accuracy of parameter estimation. To validate the potential of the model and the role of genomic information, we used real genomic data from citrus breeding materials and simulated their vegetative growth curves. In these simulations, we compare the estimation accuracy of several methods and scenarios using fragmented longitudinal data. Furthermore, we assessed genomic prediction accuracy for untested individuals. Thus, we identified the potential of these methods to estimate growth curves based on short-term data for materials with varying age structures.

Results

Generating fragmented longitudinal data from genome data

The main purpose of this study was to estimate and predict growth curves from fragmented longitudinal data obtained from an age-mixed field. To accurately evaluate the estimation and prediction performance, rather than using raw data, fragmented longitudinal data were generated from artificially created longitudinal data based on the following measurement design: In this experiment, we assumed that measurements were conducted once a year over a 2-year period in a citrus breeding field. During the first measurement, trees grafted 2, 4, and 6 years ago, which were categorized as the youngest, middle, and oldest cohorts, respectively, were measured. The same trees were measured again in the second year, resulting in 6 years of longitudinal data with 2 data points per individual (Fig. 1A).

To investigate the influence of population structure on the estimation and prediction performance, two different longitudinal datasets were generated based on population composition: one from a single-family population and the other from a population of 11 families (Table 1). We refer to the former as the "single-family group" and the latter as the "multiple-family group." During the generation of fragmented longitudinal data, the multiple-family group was further divided into two different groups; "multiple-family group I" and "multiple-family group II" depending on the allocation pattern of individuals. In single-family and multiple-family Group I, all individuals were randomly assigned to three cohorts. However, in actual breeding situations, the same cross is not repeated over multiple years, resulting in all individuals derived from the same cross concentrated within a specific year. To evaluate the estimation and prediction performance under these conditions, individuals in multiple-family group II were allocated to each cohort by family. Family allocations were determined randomly for each simulation trial (iteration).

147 The generated and prepared fragmented longitudinal data are shown in Fig. 1B. Despite
148 the dynamic fluctuation caused by the measurement noise in each curve, the overall patterns of
149 both the generated and fragmented longitudinal data follow a typical logistic growth curve. The
150 phenotype data for each year formed a distribution that resembled a normal distribution owing to
151 both genomic and residual variance. Although the position of the distribution shifted upward over
152 time, the distributions of the middle and oldest cohorts overlapped significantly, indicating that
153 the generated longitudinal data began to converge at an early stage.

154 The genetic structures of all individuals used to generate the longitudinal data were
155 visualized using principal component analysis (Fig. 1C), with 11 families represented by 11
156 distinct colors. Family 11, which formed a single-family group, was concentrated in the top-right
157 section of the graph, whereas the 11 families that comprised the multiple-family group were widely
158 dispersed across the graph, reflecting their greater genetic diversity.

159

160 **Estimation accuracy of future/past growth using a nonlinear model**

161 To assess the difference in the estimation performance depending on the section of the
162 estimated growth curve, two different scenarios were devised (Fig. 2A). In “Scenario 1,” the
163 growth curve of the youngest cohort was estimated, while “Scenario 2” focuses on the oldest cohort,
164 allowing the evaluation estimation performance for future. (younger), and past (older) growth. In
165 Scenario 1, although the fragmented longitudinal data for the youngest cohort lacked information
166 on later growth, the middle and oldest cohorts contained longitudinal data covering the later stages
167 of growth. If the growth curve estimation for the youngest cohort can leverage information from
168 the later growth of other cohorts, estimation performance is expected to improve. Similarly,
169 estimating younger age growth using data from the oldest cohort is challenging. However, the
170 estimation performance improves if the growth curve of the oldest cohort is jointly estimated with

171 those of the other two cohorts. To validate this assumption, three estimation methods were
172 compared for each scenario: Method 1, in which the growth curve of the youngest/oldest cohort
173 was estimated from only the youngest/oldest cohort data without genomic information; Method 2,
174 in which the growth curve of the youngest/oldest cohort was estimated using data from all cohorts
175 without genomic information; and Method 3, in which the growth curve of the youngest/oldest
176 cohort was estimated using data from all cohorts with genomic information, which was expected
177 to yield the highest estimation accuracy.

178 For the estimation, the fragmented longitudinal data were fitted to a logistic model with
179 three parameters: A, B, and C. Although parameter A characterizes the later growth, parameters
180 B and C determine the dynamics of the initial growth stage. The similarity between the estimated
181 and true curves was evaluated at ages 1–7 years for each scenario using both the mean square error
182 (MSE) and Pearson's correlation coefficient (correlation coefficient), as shown in Fig. 2B.

183 In scenario 1, where the later growth of the youngest cohort was estimated, the MSEs of
184 methods 2 and 3 decreased substantially compared with method 1, particularly at ages 4–7 years
185 across all groups. While the medians of the MSE of method 3 at ages 4 to 7 years were consistently
186 smaller than those of method 2, the degree of superiority varied depending on the group (Fig. 2B
187 (a), (b), and (c)). Similarly, the estimation performance evaluated by the correlation coefficient at
188 ages 4–7 years showed the worst results for Method 1 and the best for Method 3 (Supplementary
189 Fig. 1 (a), (b), and (c)). It should be noted that the MSE for Method 1 reached as high as 8000
190 mm^2, but values beyond 100 mm^2 were not shown on the y-axis owing to its scaling.

191 In scenario 2, where the younger growth of the oldest cohort was estimated, the function
192 used to calculate the initial value for the Bayesian nonlinear model function did not work properly;
193 therefore, no growth curve was obtained for method 1. The MSE of both methods were high,
194 particularly at ages two and three (Fig. 2B (d), (e), and (f)), and the correlation coefficient was

195 relatively low at ages one and two (Supplementary Fig. 1 (d), (e), and (f)), indicating imputation
196 limitations. Similar to Scenario 1, the median MSE in Method 3 was consistently smaller than that
197 in Method 2, and the median and interquartile range of the MSE in the single-family group were
198 better than those in the other two groups.

199 Although the advantage of incorporating genomic information to improve estimation
200 performance at ages 4–7 years was confirmed to be significant in scenario 1, the magnitude of this
201 advantage was influenced by the population structure. To further investigate the relationship
202 between population and the magnitude of improvement, we defined an index called "accuracy
203 improvement." This index was calculated for each simulation iteration as follows: (estimation
204 accuracy in Method 3) minus (estimation accuracy in Method 2) for the correlation coefficient,
205 and (estimation error in Method 2) minus (estimation error in Method 3) for the MSE. Because
206 the estimation performance for Methods 2 and 3 was calculated simultaneously using the same
207 created longitudinal data in each simulation iteration, taking the difference in each iteration makes
208 it possible to evaluate the improvement in estimation performance by considering the genomic
209 information more clearly. As a result, the accuracy improvement was found to be positive in most
210 iterations and showed clear differences among groups in both the MSE and correlation coefficient.
211 Multiple-family group I showed the best results, whereas the single-family group performed the
212 worst (Fig. 2C).

213 The estimation performance of the latent parameters A, B, and C, which control the
214 overall growth behavior, was also investigated, focusing on multiple-family group II in scenario 1
215 to identify the cause of accuracy improvement. Because the results of Method 1 sometimes
216 included outliers that skewed the mean value, the estimation performance was summarized using
217 the median of 1000 iterations instead of the mean, as shown in Table 2. In scenario 1, the MSEs
218 of all parameters were confirmed to improve in methods 2 and 3, with a notable improvement in

219 methods *A* and *B* when genomic information was considered. However, in Scenario 2, although
220 the MSE of parameters *A* and *B* were higher in Method 3 than in Method 2, the magnitude of the
221 difference was not as pronounced as that in Scenario 1.
222
223 **Predicting untested progeny using the model trained on incomplete longitudinal data**
224 To date, estimation of the growth curve has been limited to individuals with phenotypic data.
225 However, by incorporating the genomic information, it was possible to predict the growth curves
226 of untested individuals (Fig. 3A). To assess the prediction performance of the model trained on
227 fragmented longitudinal data, the prediction performances of latent parameters *A*, *B*, and *C* were
228 evaluated using cross-validation. The prediction accuracy (correlation coefficient) of parameter *A*
229 was higher than those of parameters B and C across all groups, with multiple-family group II
230 showing the lowest accuracy for all parameters (Fig. 3B).
231
232 **Table 1. Number of individuals in each group**

Group	Family number										
	1	2	3	4	5	6	7	8	9	10	11
single-family group	0	0	0	0	0	0	0	0	0	0	266
multiple-family group	27	28	18	19	27	27	27	27	20	19	27

233

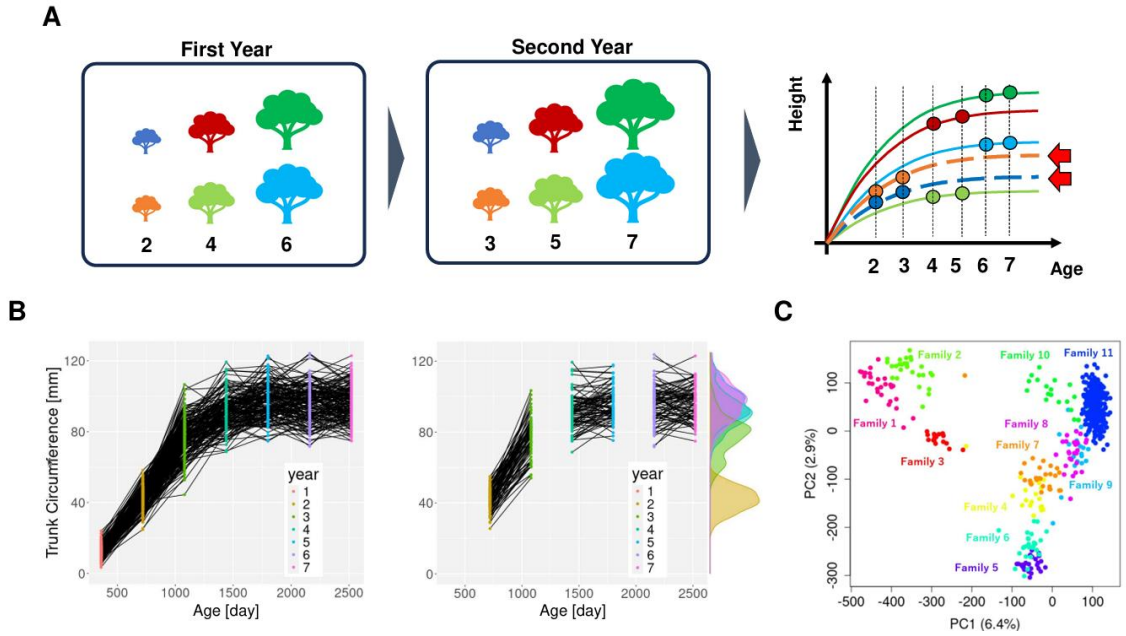

Fig. 1. Measurement design and prepared fragmented longitudinal data

(A) Detailed depiction of fragmented longitudinal data sampling and experimental scenario. The individuals with the same color are identical in the two left images, and the numbers below the trees represent the years after grafting. Measurements were conducted over 2 years for the same individuals, resulting in fragmented longitudinal data from years 2 to 7 within 2-year period. (B) Generated longitudinal data and the corresponding fragmented longitudinal data for multiple-family groups. The dots represent sampling data and are colored based on the year of sampling. (C) Principal component analysis of genomic data: all individuals were distinguished by 11 colors, corresponding to their respective families. The numbers on each axis shown in parentheses indicate the contribution rates.

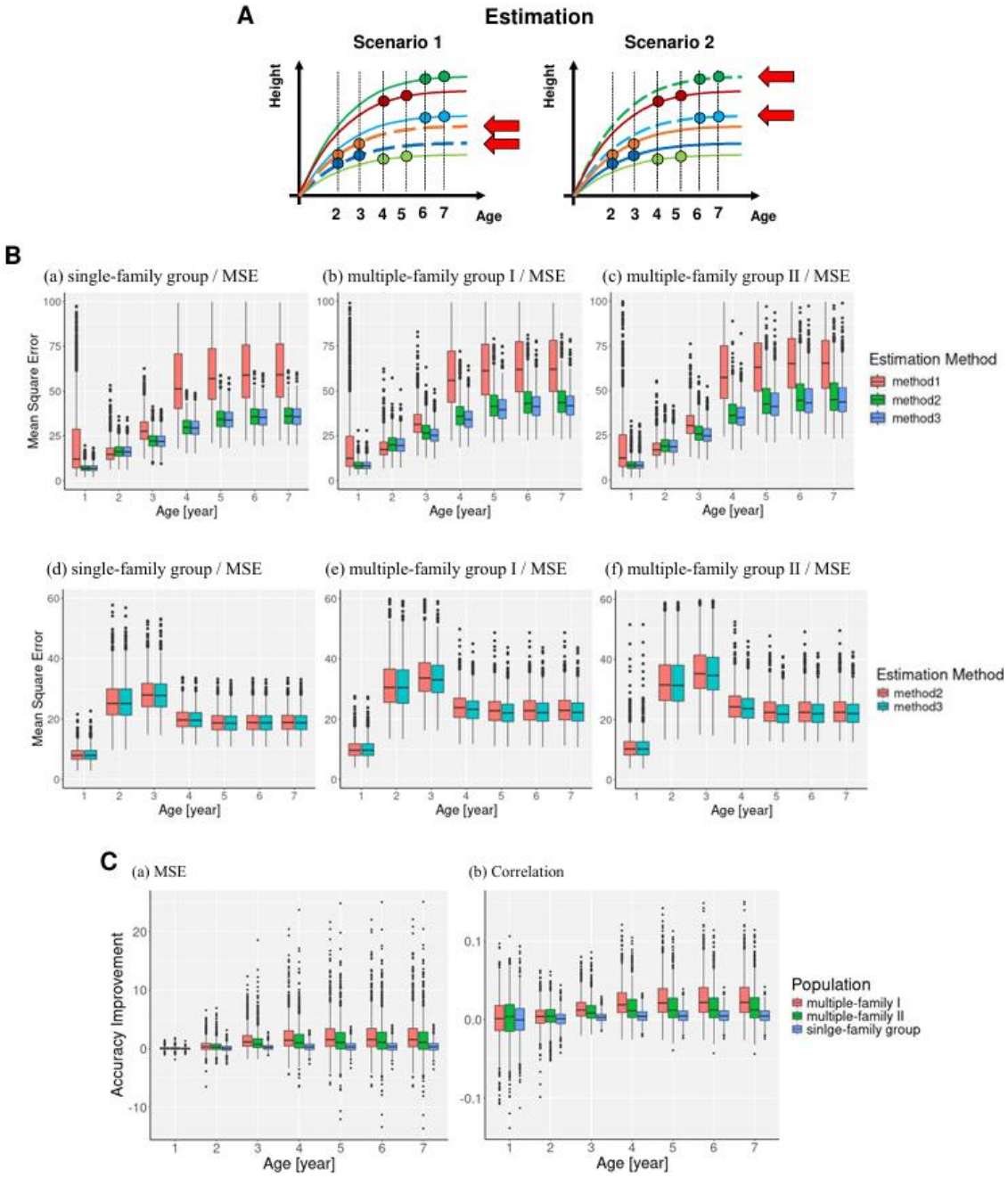

Fig. 2. Estimation scenario and estimation performance

(A) In scenario 1, the later growth of the youngest cohort was estimated using three different methods, and their estimation performance was compared. Similarly, in scenario 2, the old cohort was targeted, and the estimation performance for younger growth was compared (B) The upper three images (a), (b), and (c) show the results of scenario 1, whereas the lower three images (d),

(e), and (f) represent the results of scenario 2. Within each scenario, the left image corresponds to the single-family group, middle to the multiple-family group I, and right to the multiple-family group II. In each image, the estimation error of the growth curve was evaluated annually using the three different methods, each represented by distinct colors. Boxplots are not shown when growth curve could not be predicted. (C) Time variation of accuracy improvement: The x-axis represents the age of the growth curve, and the y-axis represents the accuracy improvement at each age. Estimation performance was evaluated using mean square error in the left image (a) and correlation coefficient in the right image (b). Accuracy improvement was compared across groups, with different colors representing each group.

Table 2. Estimation performance of each parameter

Scenario	Index	Method	Parameter		
			A	B	C
scenario 1					
	Pearson Correlation Coefficient				
		method 1	0.61	0.55	0.33
		method 2	0.62	0.56	0.32
		method 3	0.65	0.57	0.33
	Mean Square Error				
		method 1	127.9	2858.3	1733.0
		method 2	43.6	1406.1	610.6
		method 3	41.9	1399.7	611.3
scenario 2					

Pearson Correlation Coefficient

method 1	NA	NA	NA
method 2	0.65	0.00	0.00
method 3	0.65	0.02	0.01

Mean Square Error

method 1	NA	NA	NA
method 2	22.9	1722.7	657.8
method 3	22.3	1721.8	660.2

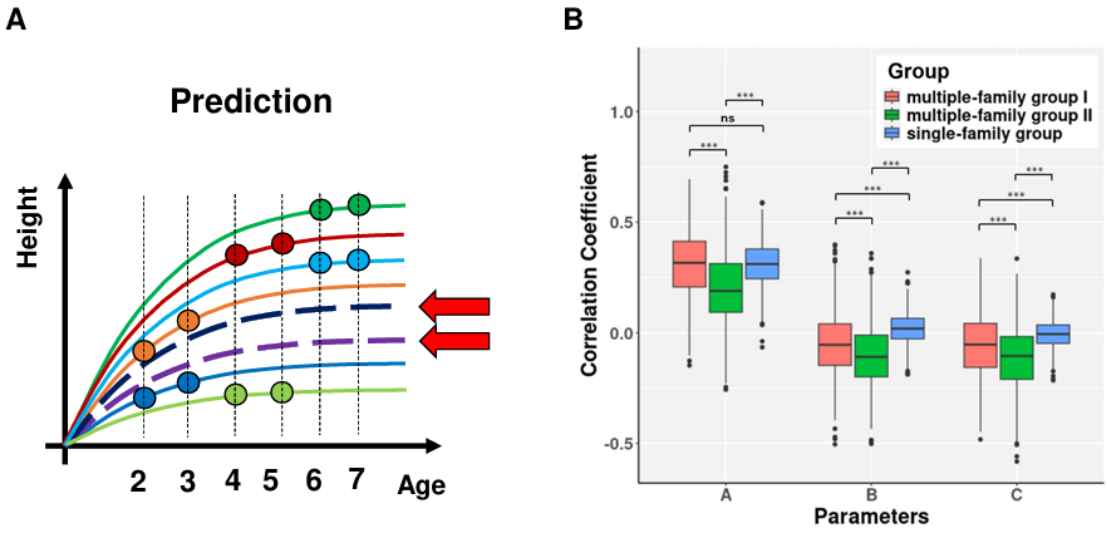

Fig. 3. Prediction scenario and prediction performance

(A) Individuals without phenotype were predicted using the model developed with fragmented longitudinal data. (B) Prediction accuracy of all parameters in the logistic model. For each parameter, the results for three different groups are represented by distinct colors. Statistical significance is indicated by asterisk: *** for $p \leq 0.001$ and ns for $p > 0.05$.

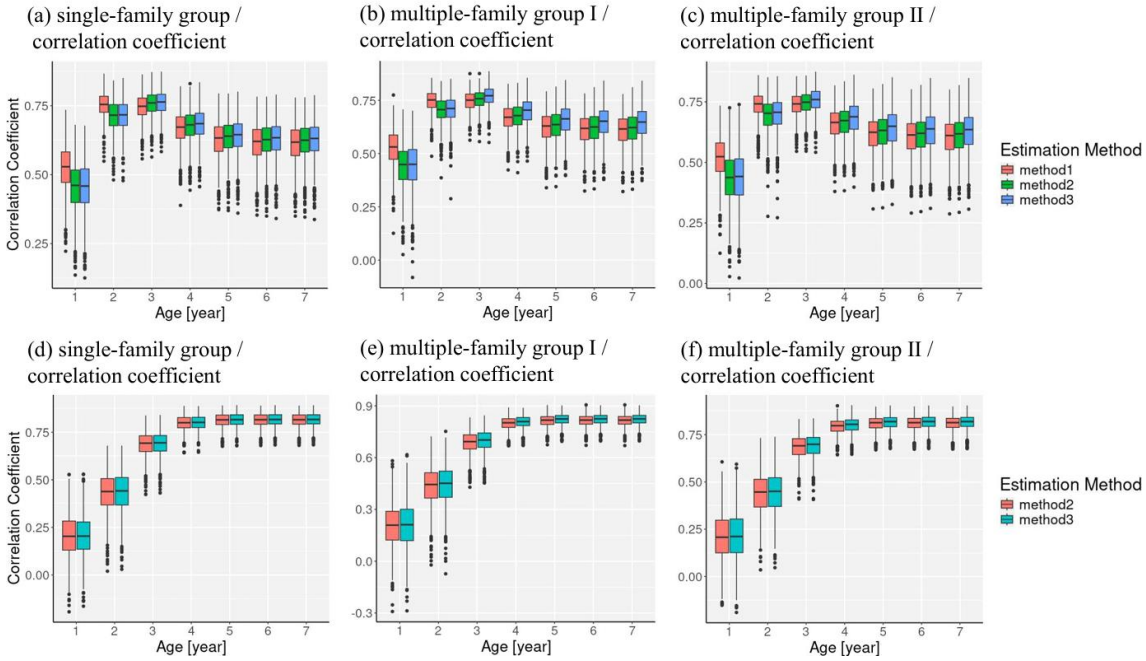

Supplementary Fig. 1. Estimation accuracy in each group

The upper three images (a), (b), and (c) show the results of Scenario 1, whereas the lower three images (d), (e), and (f) show the results of Scenario 2. Within each scenario, the left image corresponds to the single-family group, middle image to the multiple-family group I, and right image to the multiple-family group II. For each image, the estimation accuracy of the growth curve was evaluated annually using three methods, each represented by a distinct color. Box plots are not shown when the growth curve cannot be predicted.

Discussion

This study explored the feasibility of estimating the logistic growth curve from incompletely fragmented longitudinal data using a Bayesian nonlinear model to impute missing values. This approach aimed to shorten the measurement period and reduce the burden of constructing a growth curve. The fragmented longitudinal data comprised three cohorts (youngest, middle, and oldest), and the growth curve was estimated using three different methods and groups across the two scenarios. Our focus is on the following three points: 1. Extent to which the

286 estimation performance can be improved by considering data from other cohorts. 2. Whether the
287 inclusion of genomic information enhances estimation performance. 3. How population structure
288 impacts estimation performance. In addition, we evaluated the prediction performance of untested
289 individuals based on the population structure.
290
291 **Improvements by leveraging data from individuals of other cohorts**
292 A comparison of Methods 1 and 2 addressed the first question. While Method 1 requires
293 estimating the growth curve using only data from a single cohort, Method 2 enables simultaneous
294 estimation using data from all cohorts, leveraging information from individuals in other cohorts.
295 The comparison was conducted in two scenarios, and we confirmed an improvement in the
296 estimation performance for later growth in Scenario 1.
297 Method 2 in Scenario 1 was designed to enhance the estimation performance for later
298 growth, particularly for parameter A, which characterizes later growth. Interestingly, the MSEs
299 improved not only for A, but also for B and C. Although parameter A primarily represents later
300 growth, its influence extends to the initial growth phase, where B and C play critical roles.
301 Therefore, improving the estimation performance of parameter A reduces uncertainty in the initial
302 growth phase, leading to better estimates of parameters B and C. This improvement is attributed
303 to the properties of the nonlinear Bayesian model. The Bayesian nonlinear model assumes that the
304 parameters of all individuals follow the same distribution, thus preventing the parameters from
305 deviating excessively from the overall behavior. In Method 1, parameter A for the youngest cohort
306 became highly unstable due to the absence of later growth data, whereas the middle and oldest
307 cohort parameters were estimated more reliably. This assumption in the Bayesian nonlinear model
308 helps bind all the parameters together, thereby stabilizing the estimation performance for the
309 youngest cohort.

Such a function to impute missing values can be expected not only in the Bayesian nonlinear model but also in the NLMEM, where random effects are assumed to follow the same distribution. The application of the NLMEM to incomplete data with missing values has been documented in various studies[24,25]. Additionally, some studies such as ours have attempted to estimate later growth from initial growth data[32]. In a shift from plant-related research, a functional linear mixed model (FLMM) was employed in another study to estimate adult growth from children's data, using previously obtained completed longitudinal data[33]. However, our study aims to shorten the measurement period, and is distinct in that it applies specifically structured missing data, known as fragmented longitudinal data.

Meanwhile, in Method 2 of Scenario 2, in which the growth curve of the older cohort was estimated using data from all cohorts, the estimation performance of parameters B and C, which characterize initial growth, dropped below 0.5. This decline can be attributed to the exclusion of the first-year data and uniform measurement intervals. We hypothesized that the targeted growth curve would represent the trunk circumference of the scion grafted onto the rootstock. Since measuring trunk circumference in the first year is difficult due to the thinness of the trunk, the first-year data were excluded from the fragmented longitudinal data, resulting in a lack of information on the initial growth phase. Additionally, assuming annual measurements over 6 years with constant intervals led to unbalanced sampling, as reflected in the distribution shift shown in Fig. 1B, where the initial growth was not sufficiently captured. The importance of the measurement interval has been well documented in the prior research[34]. Although our study indicates that estimating initial growth from fragmented longitudinal data is challenging, the performance can be improved by adjusting the measurement intervals.

Improvement by genomic information

To explore the potential of genomic information for imputing missing values, Method 3 was designed by incorporating a genomic relationship matrix (GRM) into Method 2: Specifically, the improvement in the estimation performance by considering the GRM within the Bayesian nonlinear model was examined across three groups: the single-family group, multiple-family group I, and multiple-family group II. The superiority of Method 3 over Method 2 was confirmed, although the magnitude of superiority varied by group.

Generally, the longitudinal data at specific sampling points exhibit correlations with certain parameters. For example, late-stage longitudinal data are strongly correlated with parameter A, whereas initial-stage longitudinal data are more closely correlated with parameters B and C. Traditionally, parameter estimation has relied on these correlations. However, in this study, a large amount of data was missing, making it difficult to rely solely on correlation-based estimations. Nevertheless, when genomic information is considered, the parameters in the Bayesian nonlinear model are linked not only to phenotypes but also to genomic relationships; individuals who are genetically closer tend to have similar parameter values, and those who are genetically distant show more variation. In such cases, parameters can be estimated based on genomic relationships, which we believe will contribute to improvements in estimation performance. The algorithm for incorporating GRM into nonlinear models has been developed recently[29,30,35,36], and to the best of our knowledge, this is the first study to demonstrate the potential of genomic information for imputing missing values within a nonlinear framework.

Influence of population structure

While the inclusion of genetic information has been confirmed to improve the estimation of growth curves from fragmented longitudinal data, the magnitude of this improvement, as evaluated by accuracy, depends heavily on the group structure. Multiple-family group I showed a

358 better improvement in estimation accuracy, whereas the single-family group yielded the poorest
359 results. The key differences between these groups lie in the populations used to generate the
360 longitudinal data and the strategy for allocating individuals to the three cohorts. Because both the
361 single-family group and multiple-family group I used the same allocation strategies, their
362 estimation performances can be compared based solely on the population structure. The genetic
363 structure of the population used in this study, as visualized by PCA, clearly showed a wider range
364 of genetic variation in the multiple-family group than in the single-family group. As we are
365 evaluating the improvement guided by incorporating genomic information, a broader range of
366 genetic variation suggests great potential for improvement, which likely contributes to the higher
367 accuracy in multiple-family group I.

368 Meanwhile, multiple-family Groups I and II used the same population to generate
369 longitudinal data but applied different allocation strategies, allowing for the comparison of
370 estimation performance based solely on allocation patterns. Although the allocation strategy used
371 in multiple-family group II was more realistic, its estimation performance was lower than that of
372 multiple-family group I. When individuals are randomly assigned, as in the multiple-family group
373 I, genetically related individuals, such as those from the same family, are distributed more evenly
374 across the three cohorts, making it easier to estimate the growth curve. In contrast, when
375 individuals from the same family are concentrated in a specific cohort, such as in the multiple-
376 family group II, the phenotype data across cohorts seem less related, making it more difficult to
377 estimate phenotypic values across cohorts. In genomic selection, the prediction performance is
378 strongly influenced by the genomic relationship between the training and test populations, leading
379 to numerous studies on the impact of the allocation strategy[37]. However, the experimental setup
380 described in this section differs in that it focuses on longitudinal genetic relationships rather than
381 on the relationship between the training and test populations. Another key distinction is that this

section emphasizes estimation rather than prediction. The prediction performance considering the allocation of the training and test populations is discussed in the subsequent section.

Prediction of untested individuals

Although our primary focus has been on the estimation performance of tested individuals, the incorporation of the GRM into the Bayesian nonlinear model also enables the direct prediction of untested individuals. In this study, we attempted to build a model using fragmented longitudinal data and evaluated the prediction performance for each group. However, the prediction performance was low, particularly for parameters B and C; even parameter A did not exceed 0.4, indicating the challenge of prediction from fragmented longitudinal data.

Among the three groups, the single-family group and multiple-family group I exhibited the best prediction performance for parameter A, whereas multiple-family group II exhibited the poorest performance across all parameters. The relationship between the prediction performance and population structure has been actively studied in the context of genomic selection. For example, a previous study categorized a wheat population based on training and test population structures and found that prediction performance declined when the family of the test population was excluded from the training population, attributing the decline to the localization of family specific genes[37]. Although the prediction performances of B and C were insufficient, they may be improved by optimizing the sampling time, as mentioned earlier, which warrants further investigation.

Materials and Methods

Plant material

In this study, we used 505 individuals with different genotypes from 11 families

406 generated by the National Agriculture and Food Research Organization, Institute of Fruit Tree
407 and Tea Science (Okitsu, Shizuoka, Japan). The parents of these families had diverse backgrounds,
408 including tangerines, lemons, and pomelos, and the families were numbered from 1 to 11. Family
409 11 comprised 266 progeny, whereas the remaining 10 families had an average of 20 individuals.
410
411
412 **SNP genotyping data**
413 We conducted GRAS-Di[38] analysis using Illumina HiSeq 4000, generating 150 bp paired-
414 end reads according to the manufacturer's protocol, with an average of approximately 8 million
415 reads per sample. We then mapped the trimmed clean reads to the clementine haploid reference
416 genome v1.0
417 (https://data.jgi.doe.gov/refinedownload/phytozome?organism=Cclementina&expanded=Phyto
418 zome-182) using GSNAP (version 2021-12-17)[39] with options -k = 15 and-max-
419 mismatches=0.125, resulting in BAM files for individual samples. After sorting the BAM files in
420 coordinate order using Picard tools, the secondary mapped reads were marked and index files were
421 generated. We called polymorphic sites using the GATK4 (4.5.5.0) HaplotypeCaller and created
422 GVCF files for each sample. Next, we merged the GVCF files using GATK4 CombineGVCFs, and
423 converted the merged GVCF file into a VCF file using GATK4 GenotypeGVCFs. The VCF file
424 was filtered with thresholds of meanDP >= 20 and meanGQ >= 20 using vcftools[40]. Imputation
425 was performed using Beagle 5.2[41], selecting data based on a minor allele frequency (MAF) > 1%.
426 Using Picard, we verified the Mendelian violations in 387 trios and excluded loci with
427 inconsistencies in more than two trios. Finally, the linkage disequilibrium was calculated, and
428 SNPs were selected based on a linkage disequilibrium threshold of less than 0.95 using "LD.thin"
429 function of the R package RAINBOWR[42], resulting in a total of 45,929 makers.

430

431 **Population structure analysis**

432 Principal component analysis was performed using the SNP genotyping data of 505
433 individuals with the "prcomp" function of the R package stats.

434

435 **Longitudinal data generation**

436 The longitudinal data were generated using a growth model. Among various growth
437 models, such as the Gomperz, von Bertalanffy, and Richards models, the logistic model was best
438 suited to obtain longitudinal data of citrus trunk circumference of citrus breeding populations 2 to
439 7 years after grafting onto 3-year-old trifoliate orange rootstock (data not shown); therefore, it was
440 used in our study. The logistic model was parameterized as follows:

441 $$f(A,B,C,t) = \frac{A}{1+\exp\{-(t-B)/C\}}$$

442 where, A is the asymptotic parameter, represents the maximum value of the growth curve, B is
443 the inflection time, and $1/C$ is the growth rate at the inflection point. We assumed that these
444 parameters were unique to each individual, and the unique parameters A_i, B_i, and C_i for the i-
445 th individual were determined using the following equations:

446 $$\varphi_{i,j} = \mu_{,j} + u_{i,j}$$

447 $$\boldsymbol{u_{,j}} = \left(u_{1,j}, u_{2,j}, \ldots u_{n,j}\right)^T \sim MVN\left(0, K\sigma_{,j}^2\right)$$

448 where $\varphi_{i,j}$ is the j-th parameters of i-th individual, $\mu_{,j}$ is the mean of the j-th parameters, and
449 $u_{i,j}$ is the deviation from the global mean, characterizing each individual. $\sigma_{,j}^2$ is the variance and
450 K is the genomic relationship matrix, calculated for both the single-family group and the multiple-
451 family group using the "calcGRM" function of the RAINBOWR package. In the process of data
452 generation, the mean $\mu_{,j}$ and the variance $\sigma_{,j}^2$ were first fixed, and then the individual-specific
453 parameter $\varphi_{i,j}$ was randomly generated. These parameters were applied to a logistic model to

454 determine individual-specific growth curves. The values of $\mu_{,j}$ and $\sigma_{,j}^2$ were determined to mimic
455 the actually measured citrus trunk circumference growth data as follows:

456 $$\left(\mu_{,1}, \mu_{,2}, \mu_{,3}\right)^T = (100,800,200)^T$$

457 $$\left(\sigma_{,1}^2, \sigma_{,2}^2, \sigma_{,3}^2\right)^T = (100,2500,900)^T$$

458 Data for each year from 2 to 7 years were extracted from the generated individual-specific growth
459 curves, and longitudinal data were completed by adding measurement noise. To ensure that
460 heritability (i.e., the proportion of variance explained by genetic factors) remained constant over
461 time, the variance of the longitudinal data was first calculated at each sampling point, and then the
462 magnitude of variance was adjusted to maintain a heritability of 0.5.

463

464 **Fragmented longitudinal data generation**

465 Fragmented longitudinal data were obtained from the artificially generated longitudinal
466 data. Specifically, the 4th to 7th years' data were replaced with missing values for the youngest
467 cohort, while the 2nd, 3rd and 6th, and 7th years' data were replaced with missing values for the
468 middle cohort. Similarly, the 2nd to 7th years' data were replaced with missing values for the oldest
469 cohort.

470

471 **Estimation of latent variable**

472 To estimate the three parameters, A_i, B_i, and C_i, of the logistic model, we applied a
473 Bayesian nonlinear model. Individual growth curves were estimated by incorporating these
474 parameters into the model functions. The Bayesian nonlinear model is defined as follows:

475 Let f represent a nonlinear growth model, $\boldsymbol{D}$ the model input, $\boldsymbol{\Phi}$ the model
476 parameters, $\boldsymbol{Y}$ the observations, and i the genotype index. The model can be expressed as
477 follows:

478 $$\boldsymbol{Y}_i = f(\boldsymbol{D}_i, \boldsymbol{\Phi}_i) + \boldsymbol{\varepsilon}_i$$

479 where $\boldsymbol{\varepsilon}_i$ is the error term, assumed to follow a multiple normal distribution:

480 $$\boldsymbol{\varepsilon}_i \sim MVN(\mathbf{0}, I\sigma_\varepsilon^2)$$

481 The prior distribution of the residual variances σ_ε^2 is the Jeffreys' scale-invariant prior:

482 $$p(\sigma_\varepsilon^2) \propto \frac{1}{\sigma_\varepsilon^2}$$

483 The j-th parameter of $\boldsymbol{\Phi}_i$ is regressed on genome-wide marker genotypes as:

484 $$\varphi_{i,j} = g_j(G_i, \boldsymbol{\Theta}_j, \boldsymbol{\Psi}_j) + e_{i,j}$$

485 where G_i is the marker genotypes, g_j is the whole-genome regression function, $\boldsymbol{\Theta}_j$ is the

486 regression parameters of f_j, $\boldsymbol{\Psi}_j$ is the hyperparameters of f_j, and:

487 $$e_{i,j} \sim N(0, 1/\tau_{0,j}^2)$$

488 The prior for $\tau_{0,j}^2$ follows

489 $$p(\tau_{0,j}^2) \propto \frac{1}{\tau_{0,j}^2}$$

490 In this study, we used a GBLUP model for whole-genome regression, defined as

491 $$g = \mathbf{1}\mu + \boldsymbol{u}$$

492 with priors:

493 $$p(\mu) \propto constant$$

494 $$\boldsymbol{u} \sim MVN(\mathbf{0}, K\sigma_u^2)$$

495 where K is the additive genomic relationship matrix. The prior for σ_u^2 is:

496 $$\sigma_u^2 \sim Scaled\ inverse\ schi\ square(v_u, S_u^2)$$

497 The parameters to estimate $\boldsymbol{\Theta}$ are μ, u, τ_0^2, and σ_u^2, and the hyperparameters $\boldsymbol{\Psi}$ are v_u and S_u^2.

498 For Methods 1 and 2, in which genomic information was not used, the additive genomic

499 relationship matrix K was replaced by the identity matrix I.

500 Estimation was performed using the "GenomeBasedModel" function of the

GenomeBasedModel package in R, with the initial value set by the "drm" function of the drc package[43]. In the initial value calculation, the longitudinal dataset of all individuals was treated as a single individually derived dataset. Iterations were run 1000 times for each generated dataset, and the estimation was evaluated using both Pearson's correlation coefficient and the mean square error.

Prediction of untested individuals

When genomic information is incorporated into the Bayesian nonlinear model, the estimated parameters follow a multivariate normal distribution with a variance-covariance matrix proportional to the GRM. In this case, the logistic model parameters of untested (predicted) individuals, $\boldsymbol{\varphi}_{.j_{pred}} = \left(\varphi_{1.j_{pred}}, \ldots \varphi_{n.j_{pred}}\right)^T$, can be predicted based on the genomic relationship matrix and the estimated parameters of tested (observed) individuals, $\boldsymbol{\varphi}_{.j_{obs}} = \left(\varphi_{1.j_{obs}}, \ldots \varphi_{n.j_{obs}}\right)^T$, using the following equation[44]:

$$\boldsymbol{\varphi}_{.j_{pred}} = \mathbf{1}\mu_{.j_{pred}} + K_{pred\,pred}^{-1} K_{pred\,obs}\left(\boldsymbol{\varphi}_{.j_{obs}} - \mathbf{1}\mu_{.j_{obs}}\right)$$

where $K_{pred\,pred}$ is the additive genetic relationship matrix corresponding to the predicted individuals, and $K_{pred\,obs}$ is that of the predicted and observed individuals. $\mu_{.j_{pred}}$ and $\mu_{.j_{obs}}$ are the means of the predicted and estimated parameters (i.e., estimated parameters of an observed individual) respectively. In predicting $\boldsymbol{\varphi}_{.j_{pred}}$, $\mu_{.j_{pred}}$ is replaced by $\mu_{.j_{obs}}$. A growth curve was then constructed using these parameters.

To evaluate the prediction performance of the model constructed using the fragmented longitudinal data, we conducted the following experiment: For the single-family and multiple-family group I, one eleventh of the individuals were used as the training population, and the rest

were used as the training population, which was further divided into three cohorts. Cross-validation was performed by rotating the test population 11 times and the prediction performance was calculated. This process was repeated 1000 times using different longitudinal data. In the case of multiple-family group II, individuals were allocated by family, and each family was selected as the test population for each rotation. It should be noted that because all individuals across the three cohorts were used for growth curve prediction, there was no distinction between Methods 1 and 2.

Significance test of the difference in prediction performance

Because the variance in prediction performance across all simulation iterations differed by group, a statistical significance test for prediction performance was conducted using the Steel-Dwass asymptotic test. This was implemented with the "pSDCFlig" function in "NSM3" package in R.

Acknowledgments

We are grateful to all members of the National Agriculture and Food Research Organization Institute of Fruit Tree and Tea Science for maintaining the Citrus trees, as well as Kosuke Hamazaki and Kengo Sakurai for sharing their expertise in the simulation analysis. This research is supported by a grant from MAFF commissioned project study on "Smart breeding technologies to Accelerate the development of new varieties toward achieving "Strategy for Sustainable Food Systems, MIDORI"" and Japan Science and Technology Agency – OPERA (Program on Open Innovation Platform with Enterprises, Research Institute and Academia) Grant Number JPMJOP1851.

Data Availability Statements

Data available on request.

Conflict of interests

The authors declare that they have no conflict of interest.

Competing financial interests

The authors declare no competing financial interests.

Author Contributions

S. K. and H. I. conceived and designed the study. K.N. designed the study. T.S. extracted DNA and performed SNP genotyping. S.K., M.F.M., T.S., H.I., and K.N. conducted phenotyping. S. K. performed the simulations. H.I. provided technical help for statistical analysis. S. K. and T. S. drafted the manuscript. All the authors have read and approved the manuscript.

References

1 Yamaki S. Metabolism and accumulation of sugars translocated to fruit and their regulation. *J Japan Soc Hotic Sci* 2010; **79**: 1–15.

2 Koch KE. Translocation of photosynthetic products from source leaves to aligned juice segments in Citrus fruit. *HortScience* 1984; **19**: 260–261.

3 Koch KE. The path of photosynthate translocation into citrus fruit. *Plant Cell Environ* 1984; **7**: 647–653.

4 Rosati A, Paoletti A, Pannelli G, Famiani F. Growth Is Inversely Correlated with Yield Efficiency across Cultivars in Young Olive (Olea europaea L.) Trees. *HortScience* 2017; **52**: 1525–1529.

5 Kumar D, Srivastava KK, Singh SR. Correlation of trunk cross sectional area with fruit yield, quality and leaf nutrient status in plum under North West Himalayan region of India. *J Hortic Sci* 2019; **14**: 26–32.

6 Fagherazzi AF *et al.* Initial crown diameter influences on the fruit yield and quality of strawberry Pircinque. *Agronomy (Basel)* 2021; **11**: 184.

7 Wang Zhijunand Lan PASF. Correlation Research on the Structure of the Apple Tree Vigor and Its Fruit Quality. In: Nakamatsu Kazumiand Kountchev RAAAAE-BNAHB (ed). *New Developments of IT, IoT and ICT Applied to Agriculture*. Springer Singapore: Singapore, 2021, pp 55–63.

8 Watson A *et al.* Speed breeding is a powerful tool to accelerate crop research and breeding. *Nature Plants* 2018; **4**: 23–29.

9 Mitani N, Matsumoto R, Yoshioka T, Kuniga T. Citrus hybrid seedlings reduce initial time to

585 flower when grafted onto shiikuwasha rootstock. *Sci Hortic (Amsterdam)* 2008; **116**: 452–455.

586 10 DeBuse CJ, Shaw DV, DeJong TM. Response to inbreeding of early seedling growth and fruit
587 traits in a Prunus domestica l. Breeding population. *Acta Hortic* 2013; : 87–95.

588 11 Omura M, Shimada T. Citrus breeding, genetics and genomics in Japan. *Breed Sci* 2016; **66**:
589 3–17.

590 12 Shimizu T. Citrus breeding 2.0: A novel approach integrating deciphered parentage and
591 genomics-assisted selection. *Jpn Agric Res Q* 2019; **53**: 81–85.

592 13 Zimmerman DL *et al.* Parametric modelling of growth curve data: An overview. *Test (Madr)*
593 2001; **10**: 1–73.

594 14 Carey VJ, Wang Y-G. Mixed-effects models in S and S-plus. *J Am Stat Assoc* 2001; **96**: 1135–
595 1136.

596 15 Salas-Eljatib C, Mehtätalo L, Gregoire TG, Soto DP, Vargas-Gaete R. Growth equations in
597 forest research: Mathematical basis and model similarities. *Curr For Rep* 2021; **7**: 230–244.

598 16 Zadravec P, Veberic R, Stampar F, Schmitzer V, Eler K. Fruit Growth Patterns of Four Apple
599 Cultivars Using Nonlinear Growth Models. .

600 17 Pong-Wong R, Hadjipavlou G. A two-step approach combining the Gompertz growth model
601 with genomic selection for longitudinal data. *BMC Proc* 2010; **4 Suppl 1**: S4.

602 18 Toda Y *et al.* Genomic prediction of green fraction dynamics in soybean using unmanned
603 aerial vehicles observations. *Front Plant Sci* 2022; **13**: 828864.

604 19 Duan X *et al.* Genome-wide association analysis of growth curve parameters in Chinese
605 Simmental beef cattle. *Animals (Basel)* 2021; **11**: 192.

606 20 Xia H *et al.* Genome-wide association study of multiyear dynamic growth traits in hybrid
607 Liriodendron identifies robust genetic loci associated with growth trajectories. *Plant J* 2023;
608 **115**: 1544–1563.

609 21 Yin X, Kropff MJ, Stam P. The role of ecophysiological models in QTL analysis: the example
610 of specific leaf area in barley. *Heredity (Edinb)* 1999; **82**: 415–421.

611 22 Chang A, Yeom J, Jung J, Landivar J. Comparison of canopy shape and vegetation indices of
612 citrus trees derived from UAV multispectral images for characterization of citrus greening
613 disease. *Remote Sens (Basel)* 2020; **12**: 4122.

614 23 Moe KT, Owari T, Furuya N, Hiroshima T, Morimoto J. Application of UAV photogrammetry
615 with LiDAR data to facilitate the estimation of tree locations and DBH values for high-value
616 timber species in northern Japanese mixed-wood forests. *Remote Sens (Basel)* 2020; **12**: 2865.

617 24 Huang S, Meng SX, Yang Y. Assessing the goodness of fit of forest models estimated by
618 nonlinear mixed-model methods. *Can J For Res* 2009; **39**: 2418–2436.

619 25 Yang Y, Huang S. Comparison of different methods for fitting nonlinear mixed forest models
620 and for making predictions. *Can J For Res* 2011; **41**: 1671–1686.

621 26 Lindstrom MJ, Bates DM. Nonlinear Mixed Effects Models for Repeated Measures Data.
622 1990.

623 27 Lee SY. Bayesian nonlinear models for repeated measurement data: An overview,
624 implementation, and applications. *Mathematics* 2022; **10**: 898.

625 28 Ibrahim JG, Molenberghs G. Missing data methods in longitudinal studies: a review. *Test*
626 *(Madr)* 2009; **18**: 1–43.

627 29 Onogi A *et al.* Toward integration of genomic selection with crop modelling: the development
628 of an integrated approach to predicting rice heading dates. *Züchter Genet Breed Res* 2016;
629 **129**: 805–817.

630 30 Delattre M, Toda Y, Tressou J, Iwata H. Modeling soybean growth: A mixed model approach.
631 bioRxiv. 2024; : 2023.06.13.544713.

632 31 Gianola D, Weigel KA, Krämer N, Stella A, Schön C-C. Enhancing genome-enabled
633 prediction by bagging genomic BLUP. *PLoS One* 2014; **9**: e91693.

634 32 Hall DB, Bailey RL. Modeling and Prediction of Forest Growth Variables Based on Multilevel
635 Nonlinear Mixed Models. *For Sci* 2001; **47**: 311–321.

636 33 Ran M, Yang Y. Optimal estimation of large functional and longitudinal data by using
637 Functional Linear Mixed Model. *Mathematics* 2022; **10**: 4322.

638 34 Timmons AC, Preacher KJ. The Importance of Temporal Design: How Do Measurement
639 Intervals Affect the Accuracy and Efficiency of Parameter Estimates in Longitudinal
640 Research? *Multivariate Behav Res* 2015; **50**: 41–55.

641 35 Campbell MT, Grondin A, Walia H, Morota G. Leveraging genome-enabled growth models
642 to study shoot growth responses to water deficit in rice. *J Exp Bot* 2020; **71**: 5669–5679.

643 36 Yu H, van Milgen J, Knol E, Fernando R, Dekkers J. 307. A Bayesian hierarchical model to
644 integrate a mechanistic growth model in genomic prediction. In: *Proceedings of 12th World*
645 *Congress on Genetics Applied to Livestock Production (WCGALP)*. Wageningen Academic
646 Publishers, 2022, pp 1290–1293.

647 37 Norman A, Taylor J, Edwards J, Kuchel H. Optimising genomic selection in wheat: Effect of
648 marker density, population size and population structure on prediction accuracy. *G3*
649 *(Bethesda)* 2018; **8**: 2889–2899.

650 38 Enoki H, Takeuchi Y, Suzuki K. New genotyping technology, GRAS-Di, using next generation
651 sequencer. In: *Proceedings of the Plant and Animal Genome Conference XXVI*. 2018.

652 39 Wu TD, Reeder J, Lawrence M, Becker G, Brauer MJ. GMAP and GSNAP for genomic
653 sequence alignment: Enhancements to speed, accuracy, and functionality. *Methods Mol Biol*
654 2016; **1418**: 283–334.

655 40 Danecek P *et al.* The variant call format and VCFtools. *Bioinformatics* 2011; **27**: 2156–2158.

656 41 Browning BL, Browning SR. A unified approach to genotype imputation and haplotype-phase
657 inference for large data sets of trios and unrelated individuals. *Am J Hum Genet* 2009; **84**:
658 210–223.

659 42 Hamazaki K, Iwata H. Rainbow: Haplotype-based genome-wide association study using a
660 novel SNP-set method. *PLoS Comput Biol* 2020; **16**. doi:10.1371/journal.pcbi.1007663.

661 43 Ritz C, Baty F, Streibig JC, Gerhard D. Dose-response analysis using R. *PLoS One* 2015; **10**.
662 doi:10.1371/journal.pone.0146021.

663 44 Hallander J, Waldmann P, Wang C, Sillanpää MJ. Bayesian inference of genetic parameters
664 based on conditional decompositions of multivariate normal distributions. *Genetics* 2010;
665 **185**: 645–654.

666